Rovibrational Energies of the Hydrocarboxyl Radical from a RCCSD(T) Study

M. Mladenovic

Rovibrational Energies of the Hydrocarboxyl Radical from a RCCSD(T) Study

Mirjana Mladenović*
Université Paris-Est, Laboratoire Modélisation et Simulation Multi Echelle, MSME UMR 8208 CNRS, 5 bd Descartes, 77454 Marne la Vallée, France
(Dated: April 2, 2013)

A RCCSD(T)/cc-pVQZ potential energy surface is constructed for the HOCO radical in the ground electronic state and used to compute rotation-vibration levels of HOCO and DOCO. Two numerical strategies are employed to study in detail the wavefunction properties. The importance of stretch-bend coupling, such as ν_4/ν_5 and ν_3/ν_4, for the internal dynamics is demonstrated. The rotational constants computed for the vibrational ground state of *trans* and *cis* conformers are in good agreement with experimental values.

Keywords: hydrocarboxyl radical; rovibrational energies; intermode coupling; potential energy surface; ab initio calculation

I. INTRODUCTION

The reaction between hydroxyl radical and carbon monoxide is known to proceed via an energized HOCO intermediate,

$$\mathrm{HO} + \mathrm{CO} \rightleftharpoons \mathrm{HOCO} \rightleftharpoons \mathrm{H} + \mathrm{CO_2}. \qquad (1)$$

This was first proposed by Smith and Zellner[1,2] and later verified in photoionization,[3] ultrashort laser pulse,[4] and infrared spectroscopic studies.[5,6] The process of Eq. (1) provides the most common pathway for atmospheric depletion of both OH and CO and is the principal source of heat in hydrocarbon flames.[7,8] It is also known that the reaction of Eq. (1) exhibits a significant non-statistical (non-Arrhenius) behaviour.[9–12]

The stability of the HOCO radical was first observed in a low-temperature CO matrix isolation study of Milligan and Jacox.[13] These authors showed the existence of two geometric isomers, *trans*- and *cis*-HOCO, and assigned five fundamental transitions. Later studies in an Ar matrix[14] concluded that *trans*-HOCO is more stable than *cis*-HOCO. The first gas phase detection of HOCO is due to Ruscic *et al*,[3] who found in a photoionization mass spectrometric study that HOCO is bound by 10.2 kcal/mol (3600 cm^{-1}) with respect to the lowest energy dissociation products, H+CO_2.

Experimental spectroscopic parameters of HOCO are still scarce in the literature. High resolution gas phase data are available for the vibrational ground state,[15–17] the fundamental ν_2 (C=O stretching) vibration,[18] and the fundamental ν_1 (H-O stretching) vibration[19,20] of *trans*-HOCO and *trans*-DOCO. The first high-resolution spectra for *cis*-HOCO and *cis*-DOCO were obtained only recently. By means of Fourier transform microwave spectroscopy, Oyama *et al.*[21] recorded in total 25 lines for *cis*-HOCO and 46 lines for *cis*-DOCO, both in the vibrational ground state, and derived spectroscopic parameters of high accuracy. Recent photoelectron spectra due to Johnson *et al.*[22] provide the first gas phase observation of the low-frequency in-plane modes for both conformers of HOCO and DOCO.

In the theoretical front, a great deal of work has been focused on the curious kinetic behaviour of the reaction of Eq. (1).[12] Several global potential energy surfaces were constructed for reaction dynamics investigations.[23–27] The potential energy surface of Schatz, Fitzcharles, and Harding,[23] which went through several iterations,[25,28,29] was used also for bound state calculations carried out by means of a five-dimensional approch,[30] a MULTIMODE approach,[31], and by numerically exact full-dimenional strategies.[32,33] Botschwina[34] calculated the equilibrium structures of both *trans*-HOCO and *cis*-HOCO at the level of the spin restricted coupled cluster theory and made predictions for the ground-state rotational constants of *cis*-HOCO that agree well with the experimental results published six years later.[21] Spectroscopic properties of HOCO were studied in detail by Fortenberry *et al.* who recently developed separate quartic force fields for *trans*-HOCO [Ref. 35] and for *cis*-HOCO [Ref. 36], which were used to compute the fundamental frequencies, ground-state rotational constants, and centrifugal distortion constants by means of vibrational second order perturbation theory and vibrational configuration interaction. These force fields were reused in combination with a 6181-term RCCSD/aug-cc-pVTZ dipole moment surface to compute MULTIMODE infrared intensities for vibrational transitions of less than 4000 cm^{-1}.[37] Wang *et al.*[38] presented results for some vibrational transitions up to $2\nu_1$ and their intensities, obtained by means of three numerical approaches from a 918-term UCCSD(T)-F12/aug-cc-pVTZ potential energy surface common for the two HOCO forms and a 1928-term UCCSD(T)-F12/aug-cc-pVDZ dipole moment surface.

Our own interest in HOCO arises from the new experimental information on the pure rotational spectra[21] and the low-frequency modes.[22] The primary theoretical interest was awakened by the existence of two stable isomers undergoing large-amplitude torsional motion. For the electronic ground state X^2A', we developed a new potential energy surface (PES) based on spin restricted coupled cluster calculations (Section II). The PES covers both isomers in the range of spectroscopic interest and allows consideration of large amplitude torsional motion. Vibrational and rovibrational calculations carried out by

means of two computational methodologies (Section III) are used to derive the fundamental transitions (Section IV A), the torsional levels (Section IV B), and the effective rotational constants for the vibrational ground state of the *trans* and *cis* forms of HOCO and DOCO (Section IV C).

II. POTENTIAL ENERGY SURFACE

The six-dimensional (6D) potential energy surface for the electronic ground state (X^2A') of HOCO was scanned by means of the partially spin adapted coupled cluster RCCSD(T) method including single and double excitations and perturbative corrections for triple excitations.[39–41] The correlation consistent quadruple zeta basis set, commonly abbreviated as cc-pVQZ, was used. Only valence electrons were correlated. All calculations were carried out with the MOLPRO quantum chemistry program package.[42]

The coordinate space was parametrized in terms of the bond-distance-bond-angle coordinates r_1, r_2, r_3, α, β, and τ. The three bond distances are $r_1 = r$(H-O), $r_2 = r$(O-C), and $r_3 = r$(C=O). The angles α and β stand for the two in-plane bending angles ∠HOC and ∠OCO, respectively, whereas τ denotes the dihedral angle measured from the *cis* side.

The *ab initio* points were fitted to a six-dimensional analytical expression of the form

$$V(r_1,r_2,r_3,\alpha,\beta,\tau) = \sum_{i,j,k,l,m,n} C_{ijklmn}\, s_1^i s_2^j s_3^k \times(\alpha-\alpha_{\rm ref})^l\,(\beta-\beta_{\rm ref})^m\,\cos(n\tau), \quad (2)$$

where s_i for $i = 1,2,3$ stands for the modified Morse coordinates,[43]

$$s_i = \frac{1}{a_i}\left[1 - e^{-a_i\left(r_i/r_i^{\rm ref}-1\right)}\right]. \quad (3)$$

The geometry of the torsional saddle point was chosen to define the reference geometry $\{r_1^{\rm ref}, r_2^{\rm ref}, r_3^{\rm ref}, \alpha_{\rm ref}, \beta_{\rm ref}\}$ in Eqs. (2) and (3). Optimum values for the three nonlinear parameters a_i of the Morse coordinates s_i from Eq. (3) were obtained with a Levenberg-Marquardt nonlinear least-squares algorithm.[44] For given a_i, the expansion parameteres C_{ijklmn} were determined by means of a linear least-squares procedure.

In total, 3261 RCCSD(T)/cc-pVQZ points with energies up to 10000 $\rm cm^{-1}$ above the *trans* minimum were considered. Some of the *ab initio* points previously calculated were also used.[45] For the final fitting, a weight of a ith data point of energy E_i was set to $1/(E_i+2500\,\rm cm^{-1})$, as previously done in our study of $HCCN^-$ [Ref. 46]. All parameters smaller than one and two times their standard deviation and most of the parameters smaller than three times their standard deviation were eliminated in repeated fitting cycles. In this fashion, we arrived at a functional six-dimensional expansion consisting of 191 terms. The standard deviation of the weighted 191-term expansion was 2.5 $\rm cm^{-1}$. The expansion coefficients C_{ijklmn} of this potential energy representation are summarized in Table I. The zero of the energy scale is defined as the energy of the *trans* minimum.

A. Topography of the potential energy surface

The structural parametres of *trans*-HOCO, *cis*-HOCO and the torsional saddle point τ-HOCO obtained for the present RCCSD(T)/cc-pCVQZ potential energy surface are summarized in Table II. There we also list all electron RCCSD(T)/cc-pCVQZ results due to Botschwina[34] and RCCSD(T)/CBS results due to Fortenberry *et al.*[35,36] obtained at the estimated complete basis set (CBS) limit. As seen in Table II, the optimum bond lengths and the optimum bond angles all agree within 0.009 a_0 and 0.3°, respectively. The equilibrium rotational constants A_e and B_e, C_e show agreement within respectively 0.04 and 0.002 $\rm cm^{-1}$, *i.e.* within 0.6 %.

The two-dimensional contour maps of the six-dimensional RCCSD(T)/cc-pVQZ PES are displayed in Fig. 1. The contour maps clearly show that HOCO is a planar molecule possessing *trans* and *cis* minima. The *cis* minimum is 603 $\rm cm^{-1}$ above the *trans* counterpart, as seen in Table II. The torsional saddle point at $\tau = 86.7°$ is 3270 $\rm cm^{-1}$ above the *trans* form (Table II). The minimum energy path (MEP) along the torsional coordinate is obtained by energy minimization with respect to the other five coordinates. The optimum bond distance r_2^{opt} and the optimum bond angles α_{opt} and β_{opt} exhibit only weak torsional dependences (within 0.06 a_0 and 3°) along the torsional minimum energy path in Fig. 1. For the optimum r_1 and r_3 values, we found variations within 0.01 a_0. This finding readily indicates only weak coupling between the torsion and the in-plane vibrational modes.

III. BOUND STATE CALCULATIONS

In the bound state calculations, we employed the orthogonal (diatom+diatom) coordinates $d_1, d_2, R, \theta_1, \theta_2, \chi$ and the body-fixed expression of the kinetic energy operator.[33] For HO^aCO^b, the coordinates d_1 and d_2 refer to the H-O^a and C-O^b bond lengths, R is the distance between the centers of mass of the HO^a and CO^b subunits, θ_i is the angle enclosed by the vectors $\mathbf{d}_i$ and $\mathbf{R}$ ($i = 1,2$), and χ is the out-of-plane (torsional) angle. The body-fixed z axis is chosen to be aligned with the vector $\mathbf{R}$.[33] The (diatom+diatom) coordinates are particularly well suited to describe the dissociation of HOCO into the channel HO+CO.

For the rovibrational calculations, two numerical approaches were used, both employing a discrete variable representation (DVR) and a parity-adapted rotational-angular basis set. These methods involve no dynamical approximations and no re-expansion of the potential en-

TABLE I: Expansion coefficients C_{ijklmn} (in atomic units) of Eq. (2) for the six-dimensional RCCSD(T)/cc-pVQZ potential energy surface developed in the present work for the ground electronic state of HOCO. The reference geometry is given by $r_1^{\rm ref} = 1.82357$ a_0, $r_2^{\rm ref} = 2.57782$ a_0, $r_3^{\rm ref} = 2.22459$ a_0, $\alpha_{\rm ref} = 108.623^\circ$, and $\beta_{\rm ref} = 129.433^\circ$. The exponential parameters $a_1 = 0.4026$, $a_2 = 0.8738$, and $a_3 = 1.6075$ are used for the Morse coordinates s_1, s_2, and s_3 of Eq. (3), respectively.

$ijklmn$	C_{ijklmn}	$ijklmn$	C_{ijklmn}	$ijklmn$	C_{ijklmn}	$ijklmn$	C_{ijklmn}
000000	0.00836781	100001	-0.00745361	000101	-0.00126955	001101	-0.00725039
100000	-0.00055379	100002	-0.00087982	000102	0.00279844	001102	0.00257248
200000	0.85755655	100003	0.00003830	000103	0.00069418	001110	-0.05265608
300000	-1.59305128	200001	-0.00841369	000201	-0.00043392	001111	0.02151180
400000	1.88261547	200002	-0.00390640	000202	0.00707674	010011	0.00608270
500000	-1.92454109	300001	-0.01426951	000203	-0.00044319	010012	-0.00818092
600000	1.44273034	011000	0.51319721	000204	-0.00036894	010021	-0.08304211
700000	-0.67158588	012000	-0.29725722	000301	-0.00090028	010101	-0.00241730
010000	0.02468718	021000	-0.08194301	000302	-0.00160687	010102	-0.00570724
020000	1.07225123	010100	0.12523030	000401	0.00446180	010103	-0.00529202
030000	-2.90735982	010200	-0.07700392	000402	-0.00228362	010110	-0.01036017
040000	1.72442690	010300	0.04800357	000501	-0.00295305	010120	0.36342201
050000	1.55371903	020100	-0.13062138	000011	-0.00943983	010130	-0.50925160
060000	-1.38833909	020200	-0.07501467	000012	0.00277347	010201	-0.00662024
001000	-0.00119757	020300	0.13649482	000013	0.00049530	010202	-0.02211013
002000	2.32154526	030100	-0.31949891	000014	0.00019359	010301	0.01981882
003000	-2.72709885	030200	0.18828323	000021	0.00273316	011001	-0.00248425
004000	1.05170410	010010	0.11764941	000022	-0.00427681	011002	-0.00683282
005000	-0.57951955	010020	-0.25158541	000031	-0.00502948	011010	-0.50042611
000100	0.00296966	020010	-0.20297505	000032	0.00217071	011011	-0.02847034
000200	0.07610313	010001	0.00636039	111000	0.04613353	011100	0.00732831
000300	-0.03567142	010002	0.02414256	000111	-0.03646118	020011	0.17384948
000400	-0.00610234	010003	0.00024572	000112	-0.00228122	020101	0.02813291
000500	-0.00156040	010004	-0.00093246	000113	0.00141805	020110	0.56411952
000600	0.00406369	020001	-0.00364918	000121	-0.00872518	020111	0.62953502
000700	-0.00244732	020002	-0.01526453	000122	0.00186631	030011	-0.43577789
000800	0.00083233	030001	-0.01473643	000131	0.02191070	100011	-0.02483552
000010	0.00309784	030002	-0.05900073	000132	0.00828586	100012	0.00100967
000020	0.15477242	040001	0.00806554	000141	-0.04358681	100021	-0.00884712
000030	-0.05398365	001100	0.00157014	000142	-0.01440554	100101	-0.00192780
000040	0.03131505	001200	-0.01267875	000151	0.03819373	100102	-0.00381710
000050	-0.02190456	002100	-0.02414472	000211	0.01021089	100103	0.00123519
000060	-0.00321959	001010	0.08973371	000212	-0.00142220	100211	-0.10404632
000001	0.00146993	001020	-0.24588891	000221	0.01273082	100301	0.03558735
000002	-0.00635973	001001	-0.01066330	000222	0.01064010	101001	0.01065118
000003	-0.00003421	001002	-0.00175187	000231	-0.02983697	101002	0.00174893
000004	0.00012628	000110	0.00037507	000232	-0.01651322	101011	0.05226679
000005	0.00000067	000120	-0.00381365	000241	0.02951766	110001	0.03326665
110000	0.01766263	000130	0.00488718	000242	0.02458448	110002	0.00934577
120000	-0.17420096	000140	-0.01395447	000311	0.01831219	110010	0.06755521
210000	0.07719126	000210	-0.01364521	000321	-0.00418284	110011	0.13688878
101000	-0.01366984	000220	0.01794977	000322	-0.00446691	110100	-0.15156445
102000	-0.08398039	000230	-0.01764837	000411	0.00852331	110200	0.50257917
100100	0.03938215	000310	0.00692572	000412	-0.00157593	110201	-0.14569645
100200	-0.04843377	000320	0.01228029	000511	-0.00572459	111001	-0.03212341
100300	0.06579241	000420	-0.01487149	000312	0.00302460	120001	-0.03249419
200100	-0.01110065	000510	-0.00174238	001011	0.01606472	210001	0.04966861
100010	-0.01133534	000610	0.00202162	001012	0.00271731		

TABLE II: Geometric parameters of *trans*-HOCO, *cis*-HOCO, and the torsional saddle point τ-HOCO obtained for the RCCSD(T)/cc-pVQZ potential energy surface developed here and in previous theoretical studies.[34–36] The energy measured relative to the energy of the *trans* minimum is denoted by E_{rel}. The equilibrium rotational constants A_e, B_e, and C_e are additionally shown.

	trans-HOCO			*cis*-HOCO			τ-HOCO
	This work	Ref. 34	Ref. 35	This work	Ref. 34	Ref. 36	This work
τ/deg	180.0	180.0	180.0	0.0	0.0	0.0	86.72
α/deg	107.68	107.81	107.99	107.93	108.07	108.21	108.63
β/deg	127.03	127.11	126.98	130.27	130.33	130.24	129.45
r_1/a_0	1.8186	1.8174	1.8165	1.8364	1.8351	1.8348	1.8237
r_2/a_0	2.5388	2.5324	2.5307	2.5144	2.5086	2.5057	2.5776
r_3/a_0	2.2266	2.2223	2.2208	2.2364	2.2320	2.2306	2.2246
E_{rel} /cm^{-1}	0.0	0.0		603.3	610.8		3269.9
A_e /cm^{-1}	5.558	5.596	5.586	4.723	4.739	4.733	4.961
B_e /cm^{-1}	0.383	0.384	0.385	0.393	0.395	0.395	0.373
C_e /cm^{-1}	0.358	0.359	0.360	0.363	0.364	0.365	0.358

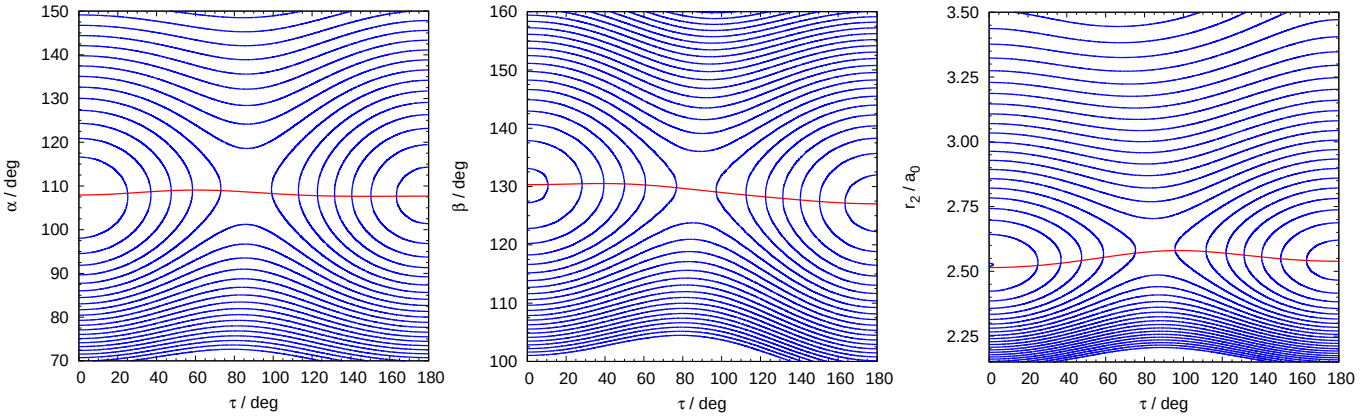

FIG. 1: Two-dimensional (τ, α), (τ, β), and (τ, r_2) contour maps of the six-dimensional RCCSD(T) PES. The remaining four coordinates are kept constant at their equilibrium values for the *trans* isomer. Contour lines are drawn in intervals of 500 cm^{-1} with the first contour placed at 250 cm^{-1}. The solid (red online) line gives the variation of the internal coordinate shown on the y axis along the torsional minimum energy path.

ergy. The DVR(6) method[47,48] is based on the discretization of the entire six-dimensional angular-radial space. The DVR(6) calculations were carried out for $J = 0$ by means of primary or/and potential optimized DVR points. The second set of calculations was performed with the help of the DVR(+R)+FBR approach,[46–48] using combined discrete variable and finite basis representations for the angular coordinates $(\theta_1, \theta_2, \chi)$ in combination with a discretized Jacobi distance R, eigenfunctions for (d_1, d_2), and symmetric top eigenfunctions for the rotational part. The DVR(6) and DVR(+R)+FBR methods both employ a contraction scheme resulting from several diagonalization/truncation steps to construct a compact basis set. The final matrix of modest size is diagonalized by standard routines, providing energies and wave functions in a simple fashion.

The DVR(6) and DVR(+R)+FBR approaches make use of several adiabatic projection schemes to study separability of (ro)vibrational motions (intermode couplings/mixing) and to characterize the exact quantum states. The computational methodology of the DVR(6) approach readily permits the construction of the adiabatic (zero-order) basis, consisting of eigenvectors computed in adiabatic torsion and in adiabatic bend approximations. The DVR(+R)+FBR, on the other hand, allows easy determination of the zero-order base in the adiabatic stretch (R) approximation. The quantum state character correlation scheme[47] is employed to monitor the evolution of the adiabatic representation in both DVR(6) and DVR(+R)+FBR computational approaches.

The DVR(6) and DVR(+R)+FBR approaches use different angular basis sets (of product and nonproduct type, respectively) and consider the contributions to the vibrational Hamiltonian in different order (different diagonalization/truncation schemes). Due to these numerical/algorithmic differences, the two approaches provide complementary information, useful for gaining a deeper insight into the nature of internal molecular dynamics.

A. Numerical aspects

The DVR(6) calculations for $J = 0$ were performed using 20 potential optimized DVR points for each of the two bending angles (θ_1, θ_2), [13, 9, 8] potential adapted discrete points for the radial coordinates $[R, d_1, d_2]$, and 21 (20) primary DVR points in even (odd) parity for the torsional angle χ, thus, giving the primary base of 7 862 400 and 7 488 000 functions in the inversion symmetric and antisymmetric block, respectively. The potential adapted DVR points were determined for the respective reference potentials defined by the equilibrium geometry of *cis*-HOCO. Dimensions of matrices diagonalized at different steps of calculation were in range 1000-2000. The final matrix had a dimension of 6300 and 6000 in even and odd parity, respectively.

In the DVR(+R)+FBR calculations, we employed 10 potential optimized DVR points for R and 12 two-dimensional eigenfunctions for d_1, d_2, constructed for the *trans*-HOCO reference geometry. The maximum value k^{max} for the projection quantum number k of the vibrational angular momentum was 15 in $J = 0$ and 18 in $J = 4$ calculations. The integrals over the torsional angle were solved by Gauss-Chebyshev quadrature of order 31. Gauss-Legendre DVR points employed for the bending angles were determined from $P^k_{l_i^{max}}$ of $k = 0, 1, \cdots, k^{max}$ with $l_1^{max} = 30$ for θ_1 and $l_2^{max} = 60$ for θ_2, keeping only the points distributed between 50° and 180° for θ_1 and between 0° and 70° for θ_2. The primary basis included 646 680 functions for $J = 0$ and 5 800 440 for $J = 4$.

The DVR(6) and DVR(+R)+FBR results show excellent agreement: the fundamental $\nu_2, \nu_3, \nu_4, \nu_5, \nu_6$ transitions agree better than 0.04 cm^{-1}, whereas we found an agreement within 0.09 and 0.5 cm^{-1} for ν_1 of *trans*-HOCO [$n^{(0,0)} = 99$] and of *cis*-HOCO [$n^{(0,0)} = 133$].

IV. RESULTS

The (ro)vibrational levels of H/DOCO were analysed in detail by means of several adiabatic projection schemes, vibrationally averaged geometries, and a visual inspection of wavefunction nodal patterns. The different approaches helped to extract valuable informations on wavefunction properties.

The full-dimensional rovibrational energies are denoted by $E^{(J,p)}$ and the corresponding ordinal numbers by $n^{(J,p)}$ for a given total rotational angular momentum J and parity p. As usual, K stands for the quantum number for the body-fixed z-projection of J. Note that the direction of the diatom-diatom vector $\mathbf{R}$ is found to depart by at most 7° from the true principal axes of H/DOCO along the torsional minimum energy path, such that $\mathbf{R}$ provides a good approximation for the principal moment of inertia axis.

A. Vibrational transitions

The fundamental vibrational transitions calculated for the present RCCSD(T)/cc-pVQZ PES are compared in Table III with available experimental data and recent theoretical results. The high resolution gas phase data,[18–20] only available for ν_1 and ν_2 of *trans*-HOCO and *trans*-DOCO, are listed there along with the values for ν_3, ν_4, ν_5 of HOCO and for ν_3, ν_5 of DOCO from photoelectron spectroscopic studies.[22] Note that the photoelectron spectroscopic data were reported with uncertainties of ±5 cm^{-1} for ν_5 and ±10 cm^{-1} for ν_3 and ν_4. For ν_1, ν_2, and ν_6 of the *cis* isomers, the experimental data are available only from matrix isolation studies.[13,14,49,50] The theoretical results due to Johnson *et al.*[22] were obtained by means of second order vibrational perturbation theory (VPT). Since the transitions from the vibrational configuration interaction calculations of Fortenberry *et*

TABLE III: Fundamental vibrational transitions of HOCO and DOCO (in cm^{-1}) obtained in the present work, in earlier theoretical studies,[22,35,36] and in experimental studies.[13,18–20,22,49,50] The experimental results are given in the columns denoted by Expt.

	trans-HOCO			*cis*-HOCO			*trans*-DOCO			*cis*-DOCO		
	This work	Ref. 35	Expt.	This work	Ref. 36	Expt.	This work	Ref. 22	Expt.	This work	Ref. 22	Expt.
ν_1	3648	3642	3636[a]	3461	3451	3411[e]	2691	2688	2684[f]	2558	2555	2522[e]
ν_2	1863	1861	1853[b]	1825	1823	1802[e]	1859	1845	1852[b]	1829	1814	1804[e]
ν_3	1217	1217	1194[c]	1278	1284	1290[c]	1092	1081	1081[c]	1132	1121	1145[c]
ν_4	1061	1053	1048[c]	1059	1046	1040[c]	906	900		961	949	
ν_5	617	617	629[c]	600	602	605[c]	593	588	597[c]	539	535	557[c]
ν_6	507	501	508[d]	543	566		396	395	472[g]	452	454	497[g]

[a] Reference 19. [b] Reference 18. [c] Reference 22. [d] Reference 49. [e] Reference 50. [f] Reference 20. [g] Reference 13.

al.[35,36] were found to be less trustworthy compared to the VPT findings,[51] we give their VPT results in Table III.

1. *Comparison with previous theoretical and experimental work*

Our results for *trans*-HOCO and for $\nu_1, \nu_2, \nu_3, \nu_5$ of *cis*-HOCO in Table III agree within 10 cm^{-1} with the theoretical VPT values of Fortenberry and others;[35,36] for ν_4 and ν_6 of *cis*-HOCO we see deviations of 13 and 24 cm^{-1}, respectively. The agreement with the results of Wang *et al.*[38] is within 10 cm^{-1}, except for ν_1 and ν_4 of *cis*-HOCO, where the deviations are roughly 20 cm^{-1}. Comparison for DOCO with the theoretical predictions of Johnson *et al.*[22] shows agreement within 15 cm^{-1}. For the quartic force fields of Fortenberry *et al.* we computed the fundamental $[\nu_1, \nu_2, \nu_3, \nu_4, \nu_5, \nu_6]$ transitions (in cm^{-1}) of $[2690, 1859, 1088, 905, 592, 392]$ for *trans*-DOCO and $[2551, 1827, 1123, 965, 541, 467]$ for *cis*-DOCO, which agree with our values within 9 cm^{-1}, except for ν_6 of *cis*-DOCO, where we see a difference of 15 cm^{-1}.

The torsional frequencies obtained here are now compared in more detail with previous theoretical values. The harmonic torsional frequencies ω_6 for the RCCSD(T)/cc-pVQZ PES, which amount to 535 and 576 cm^{-1} for respectively *trans*-HOCO and *cis*-HOCO, are in excellent agreement with ω_6 of 536 and 578 cm^{-1} reported by Johnson *et al.*[22] or 537 and 578 cm^{-1} found by Fortenberry and others.[35,36] Our anharmonic ν_6 frequencies agree within 2 cm^{-1} with the VPT results of Johnson *et al.*[22] for both isomers of HOCO and DOCO and within 10 cm^{-1} with the results of Wang *et al.*[38] for the HOCO isomers. The agreement with the VPT results of Fortenberry *et al.*[35,36] is within 6 cm^{-1} for *trans*-HOCO and 23 cm^{-1} for *cis*-HOCO. We may, however, note that the VCI torsional transitions at 488.6 for *trans*-HOCO [Ref. 35] and at 540.2 cm^{-1} for *cis*-HOCO [Ref. 36] are smaller by respectively 13 and 26 cm^{-1} than the corresponding VPT counterparts. The same authors[37] recently reported a corrected VCI ν_6 value of 475 cm^{-1} for *trans*-HOCO, along with ν_6 of 368 cm^{-1} for *trans*-DOCO and 447 cm^{-1} for *cis*-DOCO. These VCI results for ν_6 of the HOCO and DOCO isomers are, thus, all 20-25 cm^{-1} below the corresponding DVR(6) results,[51] obtained using their quartic force fields. The discrepancy between the VPT and VCI ν_6 results was attributed[38] to the transformed quartic force fields used in the VCI computations of Refs. 35,36. However, the torsional ν_6 frequencies calculated for the quartic force fields expressed in terms of the bond-distance-bond-angle coordinates (used in the VPT calculations) are found to be smaller by only 3.2 and 3.7 cm^{-1} for respectively *trans*-HOCO and *cis*-HOCO than the DVR(6) values obtained for the Morse-cosine transformed quartic force fields (used in the VCI calculations).[51] Note that the MULTIMODE computations in the single reference approach and reaction path approach yielded comparable results for ν_6 in Ref. 38.

The ν_1 and ν_2 fundamental transitions of the *trans* isomers agree within 12 and 10 cm^{-1}, respectively, with the high resolution gas phase data.[18–20] The experimental ν_1 and ν_2 frequencies available for the *cis* radicals isolated in solid N_2[50] agree with our values within 50 and 25 cm^{-1}, respectively. In the CO matrix,[13] the bands were reported at 3316 [2456] and 1797 [1798] cm^{-1} for *cis*-HOCO [*cis*-DOCO], respectively. As seen, the interaction with CO substantially lowers the ν_1 frequency. As a result of hydrogen bonding to the CO matrix through the OH group, large shifts $\Delta\nu_1$ occur relative to the free radical situation. This can be clearly seen on the example of *trans*-HOCO, for which the ν_1 transition was observed at 3456, 3571, 3603, and 3628 cm^{-1} in solid CO,[13] N_2,[50] Ar,[14] and Ne,[49] yielding $\Delta\nu_1$ of 180, 65, 33, and 8 cm^{-1}, respectively. It is worth noting that the ratio $\nu_1(N_2)/\nu_1(CO)$, with the matrix medium shown in parentheses, calculated from the data of Refs. 13 and 50, equals to 1.03 for the isomers of both HOCO and DOCO. Using the ratio $\nu_1(gas)/\nu_1(N_2)$=1.018, valid for

both *trans*-HOCO and *trans*-DOCO, we may estimate from ν_1 in solid N_2 the ν_1 values of 3473 and 2568 cm^{-1} for free *cis*-HOCO and *cis*-DOCO, respectively. These are larger by 12 and 10 cm^{-1} than our ν_1 results in Table III.

In accord with the large $\Delta\nu_1$ shifts in solid CO, it is expected that all vibrations involving hydrogen are affected by the interaction with CO, in particular the torsion. The torsional motion should appear more confined in the CO matrix than in the free radical, with the torsional fundamental at a larger frequency in the former case. The torsional ν_6 transitions observed in the CO matrix[13] at 472 cm^{-1} for *trans*-DOCO and at 497 cm^{-1} for *cis*-DOCO are noticeably larger, by 76 and 45 cm^{-1}, than our respective theoretical values. In solid Ne[49] and in solid Ar,[14] ν_6 was reported only for *trans*-HOCO, at 508.1 and 515 cm^{-1} , respectively, in close agreement with the theoretical results in Table III. Other experimental data for ν_6 are not available.

2. Low-frequency vibrations

The low-lying in-plane vibrations ν_3, ν_4, and ν_5 of H/DOCO were characterized with the help of the zero-order functions obtained in the adiabatic bend approximation for the planar arrangements ($\chi = 0, 180°$).

In the adiabatic bend approximation, the zero-order five-mode wavefunctions $\mid k;\gamma)$ are described by the kth state of the three-dimensional stretching vibration and the γth state of the two-dimensional bending vibration.[47] The energy of the adiabatic state $\mid k;\gamma)$ is $\varepsilon_{\rm adi}$. The five-mode energies obtained including the stretch-bend coupling are designated with $\varepsilon^{(5D)}$. In the DVR(6) approach, the full-dimensional vibrational energies $E^{(J,p)}$ are computed for $J = 0$ and parity p from $\varepsilon^{(5D)}$ after the inclusion of the torsional contributions (the kinetic energy and kinetic coupling with the in-plane vibrations).

The energies $\varepsilon_{\rm adi}$, $\varepsilon^{(5D)}$, and $E^{(0,0)}$ are compared in Fig. 2 for ν_3, ν_4, and ν_5. The adiabatic expansions in terms of $\mid k;\gamma)$ for the five-mode states denoted by a, b, c, d in Fig. 2 are summarized in Table IV. The latter two-component and three-component expansions provide more than 90% of the corresponding five-mode wavefunctions. The notation used by the code for $\mid k;\gamma)$ is employed in Table IV. The adiabatic states $\mid 0;1)$, $\mid 0;2)$, and $\mid 1;0)$ arise from the θ_2, θ_1, and R motion, respectively.

The coupling between the torsion and the ν_3, ν_4, ν_5 in-plane vibrations is weak for H/DOCO, as evident by small differences (up to 3.8 cm^{-1}) between the five-mode energies $\varepsilon^{(5D)}$ and the accurate level energies $E^{(0,0)}$ in Fig. 2. On the other hand, nonadiabatic (stretch-bend mixing) effects appear very important. The levels $\varepsilon^{(5D)}$ of HOCO correlated with ν_4 and ν_5 are pushed apart with respect to $\varepsilon_{\rm adi}$ due to stretch-bend coupling. The difference $\Delta\varepsilon$ between $\varepsilon^{(5D)}$ and $\varepsilon_{\rm adi}$ amounts to -93 and +47 cm^{-1} for *trans*-HOCO and to -92 and +18 cm^{-1} for *cis*-HOCO for ν_5 and ν_4, respectively. The corresponding zero-order eigenvector mixing in Table IV amounts to about 15%. For ν_4 of *cis*-HOCO, we also see the contribution from $\mid 0;2)$ in the amount of 12%. Here the $\mid 0;2)/\mid 1;0)$ (ν_4/ν_3) mixing acts in the opposite direction from $\mid 0;1)/\mid 1;0)$ (ν_4/ν_5), leading to a smaller Δ_ε value of 18 cm^{-1} compared to the value of 47 cm^{-1} for ν_5.

For the DOCO isomers, the ν_3/ν_4 mixing becomes even more important. For ν_3 and ν_4, the differences $\Delta\varepsilon$ are found to be +83 and -68 cm^{-1} for *trans*-DOCO and +94 and -64 cm^{-1} for *cis*-DOCO. Inspection of Table IV also reveals for *trans*-DOCO nearly equal contributions from the adiabatic bending state $\mid 0;2)$ and the adiabatic stretching state $\mid 1;0)$ in the five-mode state denoted by *b*, *i.e.* ν_4. The strong resonance mixing in DOCO is due to mass effects: the frequencies (in cm^{-1}) attributed to the one-dimensional $[R, \theta_2, \theta_1]$ motions are computed to be $[923, 869, 902]$ for *trans*-DOCO and $[931, 895, 942]$ for *cis*-DOCO; to be compared with $[942, 874, 1204]$ for *trans*-HOCO and $[953, 935, 1186]$ for *cis*-HOCO.

To illustrate the importance of the ν_3/ν_4 mixing, the two-dimensional contour maps of the six-dimensional wavefunctions for the vibrational ν_3 state of *trans*-HOCO, *cis*-HOCO, *trans*-DOCO, and *cis*-DOCO are shown in Fig. 3. Whereas $\mid 0;2)$ (angular character) provides the predominant contribution to ν_3 of *trans*-HOCO, the stretching contribution from $\mid 1;0)$ to ν_3 increases from 12% for *cis*-HOCO to 45% for *trans*-DOCO to 58% for *cis*-DOCO (see Table IV). Having identified the origin of ν_3 in *trans*-DOCO as $\mid 0;2)$ in Table IV, we may assume that the origin for ν_4 of *trans*-DOCO is the zero-order stretching state $\mid 1;0)$.

It should be said that this type of analysis has led to the same conclusion regarding the properties of ν_3, ν_4, ν_5 also in the case of the quartic force fields due to Fortenberry *et al.*[35,36]. For the latter PESs, the adiabatic expansions for the five-mode states considered in Fig. 2 were found to be almost identical to the results in Table IV for the PES developed here.

The nonadiabatic effects promote normal-mode character (collective nuclear motion) for the low-frequency ν_3, ν_4, ν_5 vibrations involving both radial and bending degrees of freedom. Rotational excitation does not affect the intermode mixing in these states for both HOCO and DOCO, as seen from the corresponding adiabatic expansions calculated for $J = 0 - 4$.

3. Stretching ν_1 and ν_2 vibrations

The high-frequency ν_1 and ν_2 stretching vibrations are found to be almost insensitive to the stretch-bend coupling. This is shown in Table V, where we compare the stretching energies $\varepsilon^{(1D)}_{str}$ from the one-dimensional calculations with the corresponding five-mode energies $\varepsilon^{(5D)}$. As seen there, the two energy groups differ by at most 15 cm^{-1}. Comparison of $\varepsilon^{(5D)}$ with the accurate ν_1 and

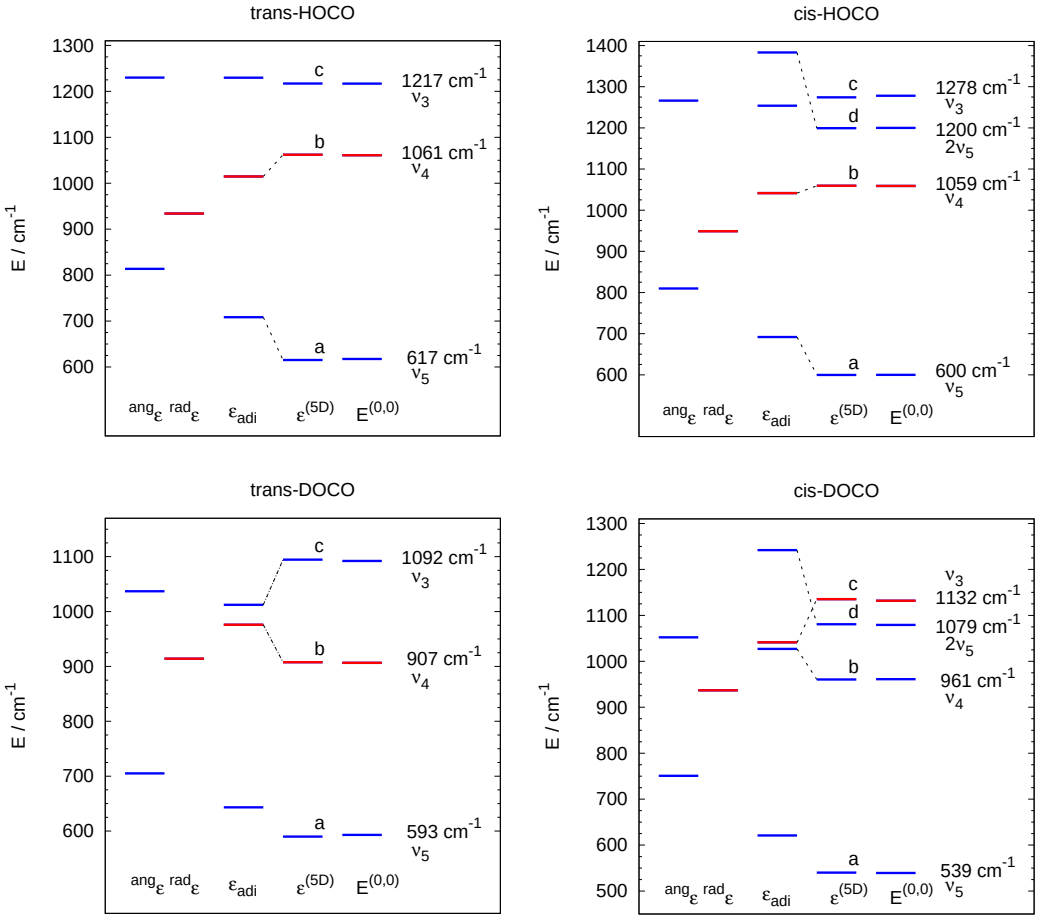

FIG. 2: Energies obtained in different stages of the DVR(6) calculation for the low-lying states of the in-plane vibrations of HOCO and DOCO. The energies calculated in the adiabatic bend approximation are denoted by $\varepsilon_{\rm adi}$, whereas $\varepsilon^{(5D)}$ and $E^{(0,0)}$ stand for the energies of the planar H/DOCO and the full-dimensional level energies, respectively. The energies ${}^{\rm ang}\varepsilon$ (${}^{\rm str}\varepsilon$) obtained using a single DVR point per radial (angular) degree of freedom are additionally shown. The adiabatic expansions for the five-mode states denoted here by a, b, c, d are listed in Table IV.

TABLE IV: Adiabatic expansions in terms of the zero-order functions $\mid k;\gamma)$ for the five-mode states $\varepsilon^{(5D)}$ denoted by a, b, c, d in Fig. 2. The zero-order function $\mid k;\gamma)$ stands for a level with k quanta in the 3D stretching vibration and γ quanta in the 2D bending vibration. The zero-order contributions underlined here are all larger than 50%. The five-mode states a, b, c, d correlate with the full-dimensional $E^{(0,0)}$ vibrational $\nu_5, \nu_4, \nu_3, 2\nu_5$ states, respectively.

$\varepsilon^{(5D)}$	$E^{(0,0)}$	*trans*-HOCO	*cis*-HOCO	*trans*-DOCO	*cis*-DOCO
a	ν_5	$\underline{0.90} \mid 0;1) + 0.40 \mid 1;0)$	$\underline{0.91} \mid 0;1) + 0.38 \mid 1;0)$	$\underline{0.93} \mid 0;1) + 0.33 \mid 1;0)$	$\underline{0.92} \mid 0;1) + 0.34 \mid 1;0)$
b	ν_4	$0.40 \mid 0;1) - \underline{0.90} \mid 1;0)$	$0.38 \mid 0;1) - \underline{0.84} \mid 1;0)$ $-0.35 \mid 0;2)$	$0.68 \mid 0;2) - 0.66 \mid 1;0)$ $+0.30 \mid 0;1)$	$\underline{0.79} \mid 0;2) - 0.53 \mid 1;0)$ $+0.26 \mid 0;1)$
c	ν_3	$\underline{0.96} \mid 0;2) - 0.07 \mid 1;0)$	$\underline{0.91} \mid 0;2) + 0.35 \mid 1;0)$ $-0.09 \mid 0;1)$	$\underline{0.72} \mid 0;2) + 0.67 \mid 1;0)$ $-0.16 \mid 0;1)$	$0.59 \mid 0;2) + \underline{0.76} \mid 1;0)$ $-0.22 \mid 0;1)$
d	$2\nu_5$		$\underline{0.82} \mid 0;3) + 0.48 \mid 1;1)$		$\underline{0.85} \mid 0;3) + 0.43 \mid 1;1)$

ν_2 energies given in Table III additionally indicates that the coupling with the torsional motion is weak.

The stretching ν_1 and ν_2 vibrations are of local-mode type, representing the H-O and C=O stretch, respectively. In agreement with this, the characterization of the states involving ν_1 and ν_2 was easily done with the help of the root mean square deviation σ_q, defined as $\sigma_q = \sqrt{\langle q^2\rangle - \langle q\rangle^2}$ for $q = d_1, d_2$.

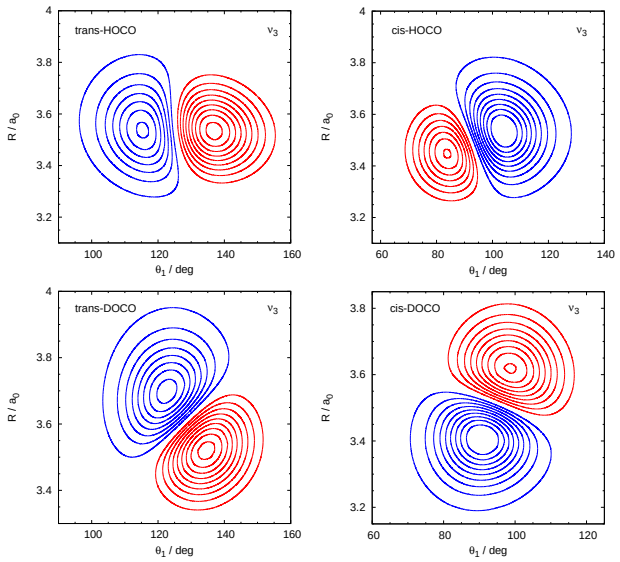

FIG. 3: Wavefunction contour maps for the vibrational ν_3 state of *trans*-HOCO, *cis*-HOCO, *trans*-DOCO, and *cis*-DOCO. The remaining four coordinates are kept constant at their equilibrium values. The contours seen in the (θ_1, R) plane show where the wavefunction takes from -95% to 95% of its maximum value with the step of 10%.

TABLE V: The fundamental high-frequency stretching transitions (in cm^{-1}) from the one-dimensional $\varepsilon_{str}^{(1D)}$ and five-dimensional $\varepsilon^{(5D)}$ calculations, keeping the remaining coordinates constant at their equilibrium values.

	trans-HOCO		*cis*-HOCO	
	$\varepsilon_{str}^{(1D)}$	$\varepsilon^{(5D)}$	$\varepsilon_{str}^{(1D)}$	$\varepsilon^{(5D)}$
ν_1	3667	3653	3474	3459
ν_2	1867	1864	1835	1824
	trans-DOCO		*cis*-DOCO	
	$\varepsilon_{str}^{(1D)}$	$\varepsilon^{(5D)}$	$\varepsilon_{str}^{(1D)}$	$\varepsilon^{(5D)}$
ν_1	2702	2693	2562	2556
ν_2	1867	1861	1835	1829

The wavefunctions corresponding to the ν_1 and ν_2 fundamentals of HOCO possess a large dominant contribution (larger than 95 %). The same was also found for the quartic force fields of Fortenberry and others.[35,36] Note that ν_1 of *cis*-HOCO was identified as a mixed state in the calculations of Wang and others.[38]

B. Torsion

The torsional motion of HOCO is described by an anharmonic double-minimum torsional potential with a non-planar barrier between the *trans* and *cis* arrangements. The expectation value $\langle\chi\rangle$ of the torsional angle is found to be about 165° and 10° in the vibrational ground state of the *trans* and *cis* isomers, respectively. It amounts to about 155° and 20° in the first excited torsional states.

HOCO levels residing either in the *trans* or the *cis* well were found by inspection of the expectation value $\langle\chi\rangle$ of the torsional angle. The extent of delocalization of the nth state is quanified with the help of the integrated wavefunction probability amplitude $P_n^{(a,b)}$,

$$P_n^{(a,b)} = \int_a^b d\chi \int |\psi_n|^2 d\Omega, \qquad (4)$$

giving the localization probability for the χ interval (a, b). In Eq. (4), Ω stands for all other coordinates. The localization probability in the *trans* well is obtained setting $a = \chi_{sp}$ and $b = 180°$, where χ_{sp} gives the position of the torsional saddle point (see Table II). In the diatom-diatom description, $\chi_{sp} = 79.1°$.

The vibrational ground state of *trans*-HOCO and the vibrational ground state of *cis*-HOCO lie at 4562 cm^{-1} and 5100 cm^{-1}, respectively. Although both ground states are placed above the electronic torsional saddle point at 3270 cm^{-1} (Table II), we found that the majority of the calculated HOCO levels are localized in one of the two wells even at high vibrational energy. This high-energy state localization can be easily understood in terms of effective (adiabatic) torsional potentials ${}^{adi}V^i = {}^{adi}V^i(\chi)$. The profiles ${}^{adi}V^i$ differ from the torsional minimum energy path in the energy of the ith state of the in-plane five-mode vibration. The barrier height ${}^{adi}E_{bar}^i$ measured with respect to the *trans* minimum of ${}^{adi}V^i$ may also differ from the corresponding MEP value. For instance, along the effective ground-state torsional profile ${}^{adi}V^0$, the *cis*-*trans* separation and ${}^{adi}E_{bar}^0$ amount respectively to 520 [548] cm^{-1} and 3109 [3135] cm^{-1} for HOCO [DOCO], being thus by 83 [55] cm^{-1} and 161 [135] cm^{-1} smaller than the corresponding electronic-potential values of 603 cm^{-1} and 3270 cm^{-1} in Table II.

The torsional saddle point on the effective ground-state profile ${}^{adi}V^0$ for HOCO is at 7410 cm^{-1}. Below this energy, there are 45 even-parity and 27 odd-parity eigenstates. Among these, 45 states are identified as strictly *trans*-HOCO states $[P_n^{(\chi_{sp},180°)} = 1]$ and 24 as strictly *cis*-HOCO states $[P_n^{(\chi_{sp},180°)} = 0]$. The remaining 3 states have a non-zero wavefunction probability amplitude in both well regions. The first tunneling *cis* state $n^{(0,0)} = 35$ at 7174 cm^{-1} and the first tunneling *trans* state $n^{(0,0)} = 36$ at 7176 cm^{-1} have $P_n^{(\chi_{sp},180°)}$ of 0.33 and 0.64, respectively. The odd-parity level $n^{0,1} = 26$ of HOCO at 7368 cm^{-1} has $P_n^{(\chi_{sp},180°)}$ of 0.24. DOCO has 69 even-parity and 45 odd-parity states below the corresponding torsional saddle point at 6773 cm^{-1} on ${}^{adi}V^0$, out of which 74 states belong strictly to *trans*-DOCO and 36 strictly to *cis*-DOCO. The remaining 4

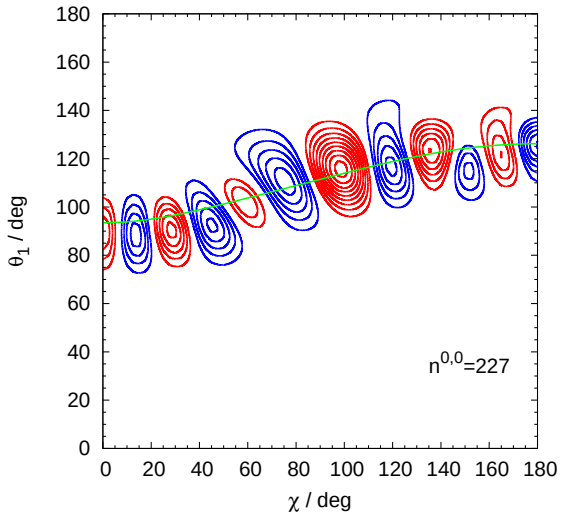

FIG. 4: Two-dimensional contour map of the full-dimensional wavefunction for the torsional even-parity state $11\nu_6$ of HOCO, obtained for the remaining four coordinates kept constant at their equilibrium values. The contours indicate where the wavefunction assumes from -95% to 95% of its maximum value with the step of 10%. The solid (green online) line shows the variation of the angle θ_1 along the torsional minimum energy path.

TABLE VI: Effective torsional frequencies (in cm^{-1}) calculated according to Eq. (5).

	trans-HOCO	*cis*-HOCO	*trans*-DOCO	*cis*-DOCO
ν_1	498	548	394	456
ν_2	505	542	396	451
ν_3	504	543	391	444
ν_4	503	530	393	448
ν_5	511	543	402	449

are tunneling states: two even-parity states at 6544 and 6581 cm^{-1} with $P_n^{(\chi_{sp},180^\circ)}$ of respectively 0.88 and 0.12 and two odd-parity states at 6719 and 6737 cm^{-1} with $P_n^{(\chi_{sp},180^\circ)}$ of respectively 0.28 and 0.90.

The tunneling states of HOCO and DOCO described in the previous paragraph are found to be pure torsional levels ($\nu_i = 0$). They lie in the vicinity of the ground state adiabatic barrier. Pure torsional states above ${}^{adi}V^0(\chi = \chi_{sp})$ are all delocalized over both minima. To illustrate this, we show in Fig. 4 the wavefunction contour map for the even-parity HOCO torsional state $11\nu_6$ lying at 9228 cm^{-1}.

The effective torsional frequency $\nu_6^{eff}(\nu_i)$ upon the excitation of the in-plane mode ν_i, estimated as the energy difference between the odd-parity and even-parity values,

$$\nu_6^{eff}(\nu_i) \;=\; E^{(0,1)}_{\nu_i+\nu_6} - E^{(0,0)}_{\nu_i}, \qquad (5)$$

are summarized in Table VI. There we see that the largest deviation of 13 cm^{-1} is between the fundamental torsional frequency from Table III and $\nu_6^{eff}(\nu_i)$ for $\nu_i = \nu_4$ of *cis*-HOCO. This is caused by the zero-order $\nu_4/2\nu_6$ mixing, as evident from the following adiabatic expansions

$$\begin{aligned} |\,\nu_4\rangle &= \underline{0.85}\,|\,2,0;0) + 0.50\,|\,0,1;0) \\ &\quad +0.11\,|\,4,0;0), \\ |\,2\nu_6\rangle &= -0.52\,|\,2,0;0) + \underline{0.84}\,|\,0,1;0) \\ &\quad +0.15\,|\,4,0;0), \end{aligned} \qquad (6)$$

whereas we have

$$|\,\nu_3\rangle \;=\; \underline{0.98}\,|\,4,0;0) - 0.18\,|\,0,1;0). \qquad (7)$$

The zero-order functions $|\,i,\alpha;p)$, computed in the adiabatic torsion approximation, describe the adiabatic levels with i quanta in the five-mode in-plane vibration and α quanta in the torsion for a given parity p. In Eq. (6), $|\,0,1;0)$=$|\,2\nu_6)$, $|\,2,0;0)$=$|\,\nu_4)$, and $|\,4,0;0)$=$|\,\nu_3)$ holds for even parity ($p = 0$). The levels $2\nu_6$, ν_4, and ν_3 are at 1041, 1059, and 1278 cm^{-1}, respectively. For the quartic force field of Fortenberry *et al*[36] for *cis*-HOCO, the $2\nu_6$ level was found to exhibit only $\nu_3/2\nu_6$ mixing (to an extent of 5%) and no $\nu_4/2\nu_6$ mixing.[51] The latter finding stems from the fact that the quartic force field of Fortenberry *et al.* supports a torsional frequency that is 21 cm^{-1} larger than ν_6 for the PES developed here. The $\nu_4, 2\nu_6, \nu_3$ levels of *cis*-HOCO and the PES of Fortenberry *et al.* are calculated to be 1046, 1099, and 1282 cm^{-1}, respectively.[51]

For the present RCCSD(T)/cc-pVQZ PES, the $\nu_4/2\nu_6$ mixing in *cis*-DOCO was found to be less pronounced (to an extent of 6%). On the other hand, $\nu_2/\nu_3 + 2\nu_6$ for *trans*-DOCO and $\nu_2/\nu_4 + 2\nu_6$ for *cis*-DOCO appear strong with a mixing of 35% and 24%, respectively.

C. Rotational constants

The rotational constants for the vibrational ground state of the *trans* and *cis* isomers of HOCO and DOCO are summarized in Table VII. Our values are obtained from $J = 0, 1$ calculations with the DVR(+R)+FBR approach. The theoretical results of Fortenberry *et al.*[35,36] were derived by means of vibrational second order perturbation theory.

The rotational constants A from the present work agree within about 30, 600, 100, and 300 MHz with the experimental finding[16,17,21] for *trans*-HOCO, *cis*-HOCO, *trans*-DOCO, and *cis*-DOCO, respectively. Our rotational constants B and C are approximately 50 MHz smaller than the experimental counterpart. With respect to the experiment, the rotational constants A due to Fortenberry *et al.* are larger by about 500 MHz and 200 MHz for respectively *trans*-HOCO and *cis*-HOCO, whereas the agreement is within 20 MHz for B and C.

TABLE VII: Rotational constants (in cm^{-1}) for the vibrational ground state of *trans*-HOCO, *cis*-HOCO, *trans*-DOCO, and *cis*-DOCO. The values in parentheses are given in MHz.

	trans-HOCO			*cis*-HOCO			*trans*-DOCO			*cis*-DOCO		
	A	*B*	*C*	*A*	*B*	*C*	*A*	*B*	*C*	*A*	*B*	*C*
theoretical results												
This work	5.5972	0.3797	0.3550	4.7476	0.3898	0.3596	5.1555	0.3550	0.3316	3.6617	0.3794	0.3432
	(167800)	(11383)	(10643)	(142328)	(11687)	(10782)	(154557)	(10642)	(9943)	(109775)	(11374)	(10289)
Refs. 35,36	5.6128	0.3819	0.3570	4.7750	0.3922	0.3618						
	(168266)	(11448)	(10702)	(143152)	(11757)	(10846)						
experimental results												
Ref. 21	5.5961	0.3814	0.3565	4.7681	0.3916	0.3612	5.1597	0.3564	0.3329	3.6726	0.3810	0.3446
	(167768)	(11433)	(10687)	(142945)	(11739)	(10830)	(154686)	(10686)	(9982)	(110100)	(11423)	(10332)
Refs. 16,17	5.5961	0.3814	0.3565				5.1598	0.3564	0.3329			
	(167766)	(11433)	(10687)				(154686)	(10686)	(9982)			

TABLE VIII: Vibrationally averaged internal geometries expressed in terms of the bond-distance-bond-angle coordinates $r_1, r_2, r_3, \alpha, \beta$ for the vibrational ground state of *trans*-HOCO, *cis*-HOCO, *trans*-DOCO, and *cis*-DOCO. The angle χ is the dihedral angle in the orthogonal diatom-diatom description. The results obtained for the present RCCSD(T) PES and for the previous quartic force fields[35,36] are shown in the columns denoted by I and II, respectively. The angles are given in degree and the distances in a_0.

	trans-HOCO		*cis*-HOCO		*trans*-DOCO		*cis*-DOCO	
	I	II	I	II	I	II	I	II
$\langle\chi\rangle$	165.0	164.8	12.3	12.1	166.5	166.4	10.7	10.6
$\langle\alpha\rangle$	107.4	107.7	107.8	108.1	107.4	107.7	107.7	108.0
$\langle\beta\rangle$	126.8	126.7	130.1	130.1	126.8	126.7	130.0	130.0
$\langle r_1\rangle$	1.854	1.853	1.875	1.873	1.845	1.843	1.864	1.862
$\langle r_2\rangle$	2.558	2.552	2.533	2.523	2.558	2.552	2.533	2.523
$\langle r_3\rangle$	2.235	2.229	2.245	2.239	2.235	2.229	2.245	2.239

For both forms of HOCO and DOCO, we give in Table VIII the vibrationally averaged geometries for the vibrational ground state obtained for the present RCCSD(T)/cc-pVQZ PES and the previous quartic force fields.[35,36] The expectation values of the bond-distance-bond-angle coordinates were obtained by their direct averaging, *i.e.* they were not evaluated from the expectation values of the orthogonal coordinates employed in the rovibrational calculations. The differences between the expectation geometries for the two PESs are comparable with the differences seen between the corresponding equilibrium structures in Table II. Comparison of Tables II and VIII shows an increase of $\langle r_1\rangle$, $\langle r_2\rangle$, and $\langle r_3\rangle$ with respect to r_1^e, r_2^e, r_3^e by about 0.035, 0.02, and 0.01 a_0, respectively. The angles $\langle\alpha\rangle$ and $\langle\beta\rangle$ are decreased with respect to α^e and β^e by 0.3° or less.

Oyama *et al.*[21] derived a r_0 structure given by (1.841 a_0, 2.536 a_0, 2.232 a_0, 107.4°, 127.4°) for *trans*-HOCO, where the internal geometry $(r_1, r_2, r_3, \alpha, \beta)$ is given in terms of the bond-distance-bond-angle coordinates. For *cis*-HOCO, they found (1.873 a_0, 2.511 a_0, 2.237 a_0, 107.3°, 131.1°). Both conformers were assumed to have a planar structure. These r_0 structures were derived also assuming the theoretical UCCSD(T)-F12/aug-cc-pVTZ values for r_2, which is thus more comparable with the value for r_2^e in Table II. Regarding the non-adjusted parameters in the r_0 structures, we note a difference of 1° for $\beta = \angle$(O-C-O) with respect to the results of Table VIII. Upon deuteration, only $\langle r_1\rangle$ in Table VIII is changed by an amount of 0.01 a_0, as assumed in Ref. 21. The contributions of the zero-point vibrations were not considered in Ref. 21.

The experimental rotational constants available for HOCO and DOCO do not provide all the information needed to derive complete experimental structures of *cis* and *trans* conformers since $I_1 = I_2 + I_3$ holds for the principal moments of inertia I_1, I_2, I_3 of planar tetratomic molecules. In other words, (at least) one of the internal coordinates has to be assumed known in a fitting procedure. After several tests, the distance r_3 was chosen to be kept constant: we used $r_3 = 2.2236\,a_0$ for *trans*-HOCO and $r_3 = 2.2335\,a_0$ for *cis*-HOCO as the mean of r_3^e from our work and Refs. 35,36 from Table II. Combining the theoretical ground-state vibrational corrections $A_e - A_0, B_e - B_0, C_e - C_0$ obtained for the RCCSD(T)/cc-pVQZ PES with the experimental ground-state rotational constants due to Oyama *et al.*[21] we finally derived the semi-experimental equilibrium r_e structure $(r_1^e, r_2^e, \alpha^e, \beta^e)$ given by (1.817 a_0, 2.534 a_0, 107.9°, 126.9°) for *trans*-HOCO and by (1.838 a_0, 2.505 a_0, 108.2°, 130.4°) for *cis*-HOCO. The latter structures

TABLE IX: Geometric parameters of selected stationary points calculated at the RCCSD(T)/cc-pVQZ level of theory. The energy measured relative to the energy of the *trans* minimum is denoted by E_{rel}.

	r_1/a_0	r_2/a_0	r_3/a_0	α/deg	β/deg	τ/deg	E_{rel} /cm^{-1}
H+CO_2		2.1971	2.1971		180.0		2150
HCO_2	2.6696	2.3125	2.3125	51.7	145.1	180	5825
HO+CO	1.8322		2.1381				9868

are in very good agreement (within 0.009 a_0 and 0.3°) with the results of Table II. Analytical expressions for the principal moments of inertia in the bond-distance-bond-angle description and their numerical partial derivatives with respect to the geometric parameters in combination with a Levenberg-Marquardt nonlinear least-squares algorithm[44] were used to compute the semi-experimental equilibrium geometry.

V. FINAL REMARKS

The RCCSD(T)/cc-pVQZ potential energy surface developed for the HOCO radical was combined with advanced strategies for the calculation of rotation-vibration levels of tetratomic molecules. Our study showed that the main features of the energy spectum of H/DOCO are large amplitude torsional motion and anharmonic mixing of the low-frequency stretch with the bending modes, whereas the coupling between the torsion and the low-frequency in-plane modes appears to be less pronounced in the region of the fundamental transitions. For a given state of the in-plane vibration, the torsional structure is found to exhibit two limiting cases associated with oscillator and rotor spectral patterns.

Several additional studies on the HOCO system are in progress. The first part is concerned with the improvement of the functional form used here to represent the potential energy surface. The analytical expansion of Eq. (2) is invariant under the spatial inversion ($\tau \rightarrow 2\pi - \tau$). However, it is not independent from the torsional angle for linear arrangements ($\alpha, \beta = 0, \pi$). These two properties of V, which are general features of any tetratomic molecule,[52] have to be combined together to obtain a physically justified potential-energy representation. Molecular arrangements with a strictly linear HOC ($\alpha = \pi$) or OHC ($\alpha = 0$) skeleton, important in the direction of the HO+CO channel over the configuration space of the weakly bound complexes HO-CO and OH-CO,[6] occur at roughly 10000 cm^{-1}. The exit channel HO+CO is also seen at this energy in Table IX. This provides an explanation why only *ab initio* points with energies up to 10000 cm^{-1} above the *trans* minimum were considered in the current fit. The further development of the PES is based on almost twice as many energy points, which have been already computed.

Ab initio points along the torsional minimum energy path were explicitly included in the fitting procedure. The number of non-planar arrangements was somewhat larger than 2000. Considering that the torsional motion above the torsional saddle point experiences a constant potential-energy contribution in the free-rotor region, we may state that our PES provides a reliable description useful for studying at least general torsional properties. In that respect, the HOCO system nicely complements the other class of tetratomic molecules, provided by the CHNO family.[53] In Table IX, we also list the optimum structure of the local minimum HCO_2, which can be related to the *trans* and *cis* forms by hydrogen migration. This is another challenge for improvements of the potential energy representation, since the two (different) oxygen atoms exposed to different interactions in HOCO become equivalent in HCO_2.

The rovibrational states of HOCO pose also a challenge for numerically exact methods. The reason for this is due to the large-amplitude torsional motion, exhibiting the onset of a rotor-like energy structure below relatively high barriers to linearity. To treat this, we need primary functions capable to capture both the one-dimensional torsional character and the rotational character of the two-dimensional vibrational angular momentum. From a practical point of view, basis sets comprising a large number of functions are required to handle the rovibrational motion of HOCO in a numerically exact fashion. We completed the rovibrational calculations for up to $J = 4$ in both parity. The results of this work, under analysis now, will be discussed in more detail elsewhere.

A final comment concerns the asymptote H+CO_2, seen at 2150 cm^{-1} above the *trans* minimum in Table IX. The ground-state energy of CO_2 is calculated to be 2536 cm^{-1} employing the CO_2 potential energy surface of Carter and Murrell[54] and our DVR-DGB approach for triatomic molecules.[55,56] In view of this estimate, states localized in the HOCO region at energies above 4686 cm^{-1} are, rigorously speaking, resonance states embedded into the continuum. For the RCCSD(T)/cc-pVQZ PES, only the ground state of *trans*-HOCO at 4562 cm^{-1} appears as a true bound state.

Acknowledgments

The author is grateful to Professor Peter Botschwina for very helpful suggestions and stimulating interest in this work.

* Corresponding author; Electronic address: mladenov@univ-mlv.fr

[1] Smith, I. W. M.; Zellner, R. Rate Measurements of Reactions of OH by Resonance Absorption. Part 2.-Reactions of OH with CO, C_2H_4 and C_2H_2, *J. Chem. Soc., Faraday Trans. 2,* **1973**, *69*, 1617–1627.

[2] Smith, I. W. The Mechanism of the OH + CO Reaction and the Stability of the HOCO Radical, *Chem. Phys. Lett.* **1977**, *49*(1), 112–115.

[3] Ruscic, B.; Schwarz, M.; Berkowitz, J. A Photoionization Study of the COOH Species, *J. Chem. Phys.* **1989**, *91*(11), 6780–6785.

[4] Scherer, N. F.; Sipes, C.; Bernstein, R. B.; Zewail, A. H. Real-Time Clocking of Bimolecular Reactions: Application to H+CO_2, *J. Chem. Phys.* **1990**, *92*(9), 5239–5259.

[5] Petty, J. T.; Harrison, J. A.; Moore, C. B. Reactions of Trans-Hydroxycarbonyl Radical Studied by Infrared Spectroscopy, *J. Phys. Chem.* **1993**, *97*(43), 11194–11198.

[6] Lester, M. I.; Pond, B. V.; Anderson, D. T.; Harding, L. B.; Wagner, A. F. Exploring the OH+CO Reaction Coordinate via Infrared Spectroscopy of the OH–CO Reactant Complex, *J. Chem. Phys.* **2000**, *113*(22), 9889–9892.

[7] Miller, J. A.; Kee, R. J.; Westbrook, C. K. Chemical Kinetics and Combustion Modeling, *Annu. Rev. Phys. Chem.* **1990**, *41*(1), 345–387.

[8] Frost, M. J.; Sharkey, P.; Smith, I. W. M. Energy and Structure of the Transition States in the Reaction OH + CO → H + CO_2, *Faraday Discuss. Chem. Soc.* **1991**, *91*, 305–317.

[9] Ravishankara, A.; Thompson, R. Kinetic Study of the Reaction of OH with CO from 250 to 1040 K, *Chem. Phys. Lett.* **1983**, *99*(5-6), 377–381.

[10] Fulle, D.; Hamann, H. F.; Hippler, H.; Troe, J. High Pressure Range of Addition Reactions of HO. II. Temperature and Pressure Dependence of the Reaction HO+CO ⇒ HOCO → H+CO_2, *J. Chem. Phys.* **1996**, *105*(3), 983–1000.

[11] Golden, D. M.; Smith, G. P.; McEwen, A. B.; Yu, C.-L.; Eiteneer, B.; Frenklach, M.; Vaghjiani, G. L.; Ravishankara, A. R.; Tully, F. P. OH(OD) + CO: Measurements and an Optimized RRKM Fit, *J. Phys. Chem. A* **1998**, *102*(44), 8598–8606.

[12] Guo, H. Quantum Dynamics of Complex-Forming Bimolecular Reactions, *Int. Rev. Phys. Chem.* **2012**, *31*(1), 1–68.

[13] Milligan, D. E.; Jacox, M. E. Infrared Spectrum and Structure of Intermediates in the Reaction of OH with CO, *J. Chem. Phys.* **1971**, *54*(3), 927–942.

[14] Jacox, M. E. The Vibrational Spectrum of the t-HOCO Free Radical Trapped in Solid Argon, *J. Chem. Phys.* **1988**, *88*(8), 4598–4607.

[15] Radford, H. E.; Wei, W.; Sears, T. J. The Rotational Spectrum of trans-HOCO and DOCO, *J. Chem. Phys.* **1992**, *97*(6), 3989–3995.

[16] Sears, T. J.; Radford, H. E.; Moore, M. A. b-Dipole Transitions in trans-HOCO Observed by Far Infrared Laser Magnetic Resonance, *J. Chem. Phys.* **1993**, *98*(9), 6624–6631.

[17] Radford, H.; Moore, M.; Sears, T.; Grussdorf, J.; Nolte, J.; Temps, F. Far-Infrared Laser Magnetic Resonance of X 2A' trans-DOCO, *J. Mol. Spectrosc.* **1994**, *165*(1), 137–149.

[18] Sears, T. J.; Fawzy, W. M.; Johnson, P. M. Transient Diode Laser Absorption Spectroscopy of the ν_2 Fundamental of trans-HOCO and DOCO, *J. Chem. Phys.* **1992**, *97*(6), 3996–4007.

[19] Petty, J.; Moore, C. Transient Infrared Absorption Spectrum of the ν_1 Fundamental of trans-HOCO, *J. Mol. Spectrosc.* **1993**, *161*(1), 149–156.

[20] Petty, J. T.; Moore, C. B. Transient Infrared Absorption Spectrum of the ν_1 Fundamental of trans-DOCO, *J. Chem. Phys.* **1993**, *99*(1), 47–55.

[21] Oyama, T.; Funato, W.; Sumiyoshi, Y.; Endo, Y. Observation of the Pure Rotational Spectra of trans- and cis-HOCO, *J. Chem. Phys.* **2011**, *134*(17), 174303.

[22] Johnson, C. J.; Harding, M. E.; Poad, B. L. J.; Stanton, J. F.; Continetti, R. E. Electron Affinities, Well Depths, and Vibrational Spectroscopy of cis- and trans-HOCO, *J. Am. Chem. Soc.* **2011**, *133*(49), 19606–19609.

[23] Schatz, G. C.; Fitzcharles, M. S.; Harding, L. B. State-to-State Chemistry with Fast Hydrogen Atoms. Reaction and Collisional Excitation in H + CO_2, *Faraday Discuss. Chem. Soc.* **1987**, *84*, 359–369.

[24] Yu, H.-G.; Muckerman, J. T.; Sears, T. J. A Theoretical Study of the Potential Energy Surface for the Reaction OH+CO → H+CO_2, *Chem. Phys. Lett.* **2001**, *349*(5-6), 547–554.

[25] Lakin, M. J.; Troya, D.; Schatz, G. C.; Harding, L. B. A Quasiclassical Trajectory Study of the Reaction OH + CO → H + CO_2, *J. Chem. Phys.* **2003**, *119*(12), 5848–5859.

[26] Valero, R.; van Hemert, M. C.; Kroes, G.-J. Classical Trajectory Study of the HOCO System Using a New Interpolated ab initio Potential Energy Surface, *Chem. Phys. Lett.* **2004**, *393*(1-3), 236–244.

[27] Li, J.; Wang, Y.; Jiang, B.; Ma, J.; Dawes, R.; Xie, D.; Bowman, J. M.; Guo, H. Communication: A Chemically Accurate Global Potential Energy Surface for the HO + CO → H + CO_2 Reaction, *J. Chem. Phys.* **2012**, *136*(4), 041103.

[28] Kudla, K.; Schatz, G. C.; Wagner, A. F. A Quasiclassical Trajectory Study of the OH+CO Reaction, *J. Chem. Phys.* **1991**, *95*(3), 1635–1647.

[29] Bradley, K. S.; Schatz, G. C. A Quasiclassical Trajectory Study of H+CO_2: Angular and Translational Distributions, and OH Angular Momentum Alignment, *J. Chem. Phys.* **1997**, *106*(20), 8464–8472.

[30] Zhang, D. H.; Zhang, J. Z. H. Quantum Calculations of Reaction Probabilities for HO + CO → H + CO_2 and Bound States of HOCO, *J. Chem. Phys.* **1995**, *103*(15), 6512–6519.

[31] Bowman, J. M.; Christoffel, K.; Weinberg, G. Calculations of Low-Lying Vibrational States of cis- and trans-HOCO, *J. Mol. Struct. (THEOCHEM)* **1999**, *461-462*(0), 71–77.

[32] Lehoucq, R.; Gray, S.; Zhang, D.-H.; Light, J. Vibrational Eigenstates of Four-Atom Molecules: A Parallel Strategy Employing the Implicitly Restarted Lanczos Method, *Computer Phys. Commun.* **1998**, *109*(1), 15–25.

[33] Mladenović, M. Rovibrational Hamiltonians for General Polyatomic Molecules in Spherical Polar Parametrization. I. Orthogonal Representations, *J. Chem. Phys.* **2000**, *112*(3), 1070–1081.

[34] Botschwina, P. Accurate Equilibrium Structures for Small Polyatomic Molecules, Radicals and Carbenes, *Mol. Phys.* **2005**, *103*(10), 1441–1460.

[35] Fortenberry, R. C.; Huang, X.; Francisco, J. S.; Crawford, T. D.; Lee, T. J. The trans-HOCO Radical: Quartic Force Fields, Vibrational Frequencies, and Spectroscopic Constants, *J. Chem. Phys.* **2011**, *135*(13), 134301.

[36] Fortenberry, R. C.; Huang, X.; Francisco, J. S.; Crawford, T. D.; Lee, T. J. Vibrational Frequencies and Spectroscopic Constants from Quartic Force Fields for cis-HOCO: The Radical and the Anion, *J. Chem. Phys.* **2011**, *135*(21), 214303.

[37] Huang, X.; Fortenberry, R. C.; Wang, Y.; Francisco, J. S.; Crawford, T. D.; Bowman, J. M.; Lee, T. J. Dipole Surface and Infrared Intensities for the cis- and trans-HOCO and DOCO Radicals, *J. Phys. Chem. A, Articles ASAP (As Soon As Publishable)* **2013**, DOI: 10.1021/jp3102546.

[38] Wang, Y.; Carter, S.; Bowman, J. M. Variational Calculations of Vibrational Energies and IR Spectra of trans- and cis-HOCO Using New ab Initio Potential Energy and Dipole Moment Surfaces, *J. Phys. Chem. A, Articles ASAP (As Soon As Publishable)* **2013**, DOI: 10.1021/jp309911w.

[39] Hampel, C.; Peterson, K. A.; Werner, H.-J. A Comparison of the Efficiency and Accuracy of the Quadratic Configuration Interaction (QCISD), Coupled Cluster (CCSD), and Brueckner Coupled Cluster (BCCD) Methods, *Chem. Phys. Lett.* **1992**, *190*(1-2), 1–12.

[40] Deegan, M. J.; Knowles, P. J. Perturbative Corrections to Account for Triple Excitations in Closed and Open Shell Coupled Cluster Theories, *Chem. Phys. Lett.* **1994**, *227*(3), 321–326.

[41] Knowles, P. J.; Hampel, C.; Werner, H.-J. Coupled Cluster Theory for High Spin, Open Shell Reference Wave Functions, *J. Chem. Phys.* **1993**, *99*(7), 5219–5227.

[42] MOLPRO, a package of ab initio programs. Werner, H.-J.; Knowles, P. J.; Knizia, G.; Manby, F. R.; Schütz, M.; Celani, P.; Korona, T.; Lindh, R.; Mitrushenkov, A.; Rauhut, G.; *et al.* see http://www.molpro.net.

[43] Meyer, W.; Botschwina, P.; Burton, P. Ab Initio Calculation of Near-Equilibrium Potential and Multipole Moment Surfaces and Vibrational Frequencies of H_3^+ and Its Isotopomers, *J. Chem. Phys.* **1986**, *84*(2), 891–900.

[44] Press, W. H.; Flannery, B. P.; Teukolsky, S. A.; Vetterling, W. T. *Numerical Recipes;* Cambridge University Press: Cambridge, 1986.

[45] Krekeler, C. *Theoretische Untersuchungen am Radikal HOCO und dem Anion HCO_2^-,* Diplomarbeit, Georg-August-Universität zu Göttingen, Institut für Physikalische Chemie, **2004**.

[46] Mladenović, M.; Botschwina, P.; Puzzarini, C. Six-Dimensional Potential Energy Surface and Rovibrational Energies of the HCCN Radical in the Ground Electronic State, *J. Phys. Chem. A* **2006**, *110*(16), 5520–5529.

[47] Mladenović, M. Discrete Variable Approaches to Tetratomic Molecules: Part I: DVR(6) and DVR(3)+DGB Methods, *Spectrochim. Acta, Part A* **2002**, *58*(4), 795–807.

[48] Mladenović, M. Efficient Calculation of Rovibrational Energy Levels of General Tetratomic Molecules by Pointwise Representation Methods, In Rollnik, H., Wolf, D., Eds., *NIC Symposium 2001*, Vol. 9 of *NIC Series*, pages 85–94, Jülich, 2002. John von Neumann Institite for Computing.

[49] Forney, D.; Jacox, M. E.; Thompson, W. E. Infrared Spectra of trans-HOCO, $HCOOH^+$, and HCO_2^- Trapped in Solid Neon, *J. Chem. Phys.* **2003**, *119*(20), 10814–10823.

[50] Mielke, Z.; Olbert-Majkut, A.; Tokhadze, K. G. Photolysis of the OC$\cdots$HONO Complex in Low Temperature Matrices: Infrared Detection and Ab Initio Calculations of Nitrosoformic Acid, HOC(O)NO, *J. Chem. Phys.* **2003**, *118*(3), 1364–1377.

[51] Mladenović, M. Vibrational Calculation for the HOCO Radical and the cis-HOCO Anion, *J. Chem. Phys.* **2012**, *137*(1), 014306.

[52] Mladenović, M. On Intervector Angle Descriptions and Their Numerical Implementation for Solving Molecular Problems, *J. Chem. Phys.* **2003**, *119*, 11513–11525.

[53] Mladenović, M.; Elhiyani, M.; Lewerenz, M. Quasilinearity in Tetratomic Molecules: an Ab Initio Study of the CHNO Family, *J. Chem. Phys.* **2009**, *130*, 154109.

[54] Carter, S.; Murrell, J. N. Analytical Two-Valued Potential Energy Functions for the Ground State Surfaces of $CO_2(\widetilde{X}^1\Sigma_g^+)$ and $CS_2(\widetilde{X}^1\Sigma_g^+)$, *Croat. Chem. Acta* **1984**, *57*, 355.

[55] Mladenović, M.; Schmatz, S. Theoretical Study of the Rovibrational Energy Spectrum and the Numbers and Densities of Bound Vibrational States for the System HCO^+/HOC^+, *J. Chem. Phys.* **1998**, *109*, 4456–4470.

[56] Mladenović, M.; Botschwina, P.; Sebald, P.; Carter, S. A Theoretical Study of the Acetylide Anion, HCC^-, *Theo. Chem. Acc.* **1998**, *100*, 134–146.

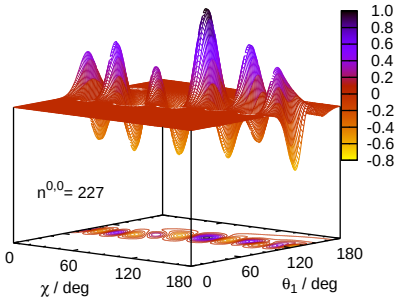
1.0
0.8
0.6
0.4
0.2
0
-0.2
-0.4
-0.6
-0.8
n^0,0 = 227
0
60
120
180
χ / deg
0
60
120
180
θ1 / deg